DOI https: //doi. org/10.1007/s11595-023-2829-7

Research on the Low-carbon Cementitious Materials: Effect of Triisopropanolamine on the Hydration of Phosphorous Slag and Steel Slag

ZHANG Ting[1], MA Baoguo[1*], XIA Yu[2]

(1. State Key Laboratory of Silicate Materials for Architectures, Wuhan University of Technology, Wuhan 430070, China; 2. School of Surveying & Testing, Shaanxi Railway Institute, Weinan 714000, China)

Abstract: Cement, phosphorous slag (PS), and steel slag (SS) were used to prepare low-carbon cementitious materials, and triisopropanolamine (TIPA) was used to improve the mechanical properties by controlling the hydration process. The experimental results show that, by using 0.06% TIPA, the compressive strength of cement containing 60% PS or 60% SS could be enhanced by 12% or 18% at 28 d. The presence of TIPA significantly affected the hydration process of PS and SS in cement. In the early stage, TIPA accelerated the dissolution of Al in PS, and the formation of carboaluminate hydrate was facilitated, which could induce the hydration; TIPA promoted the dissolution of Fe in SS, and the formation of Fe-monocarbonate, which was precipitated on the surface of SS, resulting in the postponement of hydration, especially for the high SS content. In the later stage, under the continuous solubilization effect of TIPA, the hydration of PS and SS could refine the pore structure. It was noted that compared with portland cement, the carbon emissions of cement-PS-TIPA and cement-SS-TIPA was reduced by 52% and 49%, respectively.

Key words: phosphorous slag; steel slag; high content; triisopropanolamine; hydration process; low-carbon emissions

1 Introduction

Global warming caused by the massive emission of greenhouse gas (*i e*, CO_2) has attracted more and more attention from all over the world[1,2]. Cement, the most widely used building material, accounts for 7% of global anthropogenic CO_2 emissions, while it accounts for 13.75% in China[3-5].The preparation of cementitious materials using fly ash[6], ground granulated blast furnace slag[7] and other by-products[8] as supplementary cementitious materials (SCMs) instead of cement is an important method of directly reduce CO_2 emissions[9-11].

Phosphorous slag (PS) and steel slag (SS) are industrial by-products produced in producing yellow phosphorus and steelmaking, respectively[12,13]. PS is mainly composed of CaO and SiO_2 with more than 85% glassy-phase content, proving that PS has potential activity[14]. SS comprises calcium silicates (mainly C_2S), which confirms SS has hydraulic activity[15]. However, the utilization rate of PS and SS is only 20%, and most of them are treated by stockpiling, which wastes resources, occupies land and pollutes environment[15,16]. There are some reasons that limit the large-scale utilization of PS and SS as SCMs, including retarding/inhibiting effect (because of the existence of P_2O_5, causing to the delay in setting time and the reduction in early strength) of PS and SS[17,18], and poor grindability (because of the existence of RO phase)[19,20], soundness issue (because of the existence of MgO and free CaO, and leading to the potential volumetric expansion in the later hydration period)[21,22] of SS.

Mechanical activation[12], nano-modification[23,24], chemical activation[25-27] and high temperature curing[28,29] are effective methods to improve the utilization of PS and SS and enhance the strength development in cementitious materials. Among them, chemical activation is often used due to its advantages of not increasing

(Received: Jan. 17, 2023; Accepted: Apr. 25, 2023)

ZHANG Ting(张婷): Ph D; E-mail: 290135@whut.edu.cn

*Corresponding author: MA Baoguo(马保国): Prof.; Ph D; E-mail: mbgjob@163.com

Funded by the Key Public Welfare Special Project of Henan Province (No.201300311000) and the Major Technical Innovation Project in Hubei Province of China (No.2020BED025)

CO_2 emissions and affordability. Triisopropanolamine (TIPA), a kind of alkanolamines, promotes ionic dissolution by forming TIPA-Fe chelates, and then improves the hydration degree of cement and SCMs, resulting in an increase in strength[30-32]. Therefore, combining TIPA with PS/SS may be an effective approach to increase PS/SS content in cementitious materials.

In this paper, various dosages of TIPA were added into cement-PS system and cement-SS system, and compressive strength was tested. Hydration process was measured by isothermal calorimeter. Hydration products were characterized by X-ray diffractometer (XRD) and thermogravimetric analysis (TGA). Microstructure was assessed by mercury intrusion porosimetry (MIP). The impact of TIPA on the ions dissolution of PS and SS was assessed by inductive coupled plasma emission spectrometer (ICP) and scanning electron microscope (SEM). The primary objective of this study is to offer ideas for improving the mechanical properties of low-carbon cementitious materials with high content of PS and SS.

2 Experimental

2.1 Materials

Ordinary portland cement (PI 42.5) meeting GB 175-2007 was used. Phosphorous slag (PS) and steel slag (SS) (produced in Hubei Province, China) were used, and ground with a ball mill (ϕ 500 mm×500 mm) for 30 and 40 min before use respectively. A reagent-grade TIPA ($[CH_3CH(OH)CH_2]_3N$, ⩾ 95.0% purity) was used as an admixture. Besides, properties and particle size distribution of raw materials are shown in Table 1 and Fig.1, respectively. XRD patterns of PS and SS are shown in Fig.2, and it is proved that the mineral composition of PS is mainly amorphous, except some calcium carbonate ($CaCO_3$) and magnesium oxide (MgO), and that of SS is C_2S, C_3S, and RO phase, *etc*. SEM images of PS and SS are presented in Fig.3.

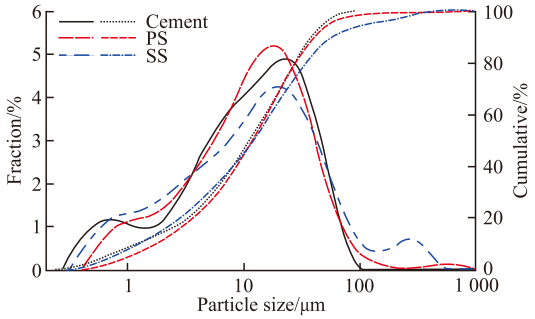

Fig.1 Particle size distribution of cement and PS

Table 1 The properties of raw materials

	Cement	PS	SS
Chemical composition/wt%			
CaO	62.58	46.78	41.18
SiO_2	20.99	35.65	14.65
Al_2O_3	5.07	4.60	3.78
Fe_2O_3	3.27	0.39	25.31
SO_3	2.34	1.47	0.51
MgO	1.90	1.34	6.19
Na_2O	0.19	0.40	0.08
K_2O	0.61	1.58	0.03
P_2O_5	0.27	3.15	1.53
MnO	0.24	-	1.42
F	-	3.23	0.51
Loss	1.91	0.56	3.45
Physical properties			
D50/μm	11.326	11.913	12.171
Density/(g/cm^3)	3.05	2.95	3.91
Specific surface area/(m^2/kg)	365	346	428

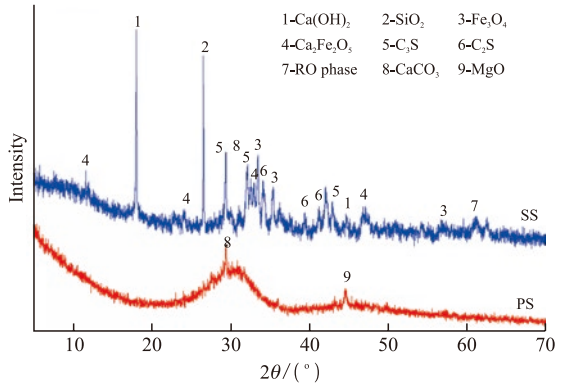

Fig.2 XRD patterns of PS and SS

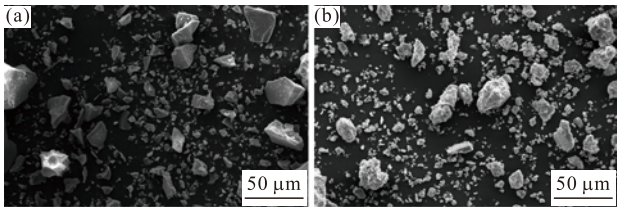

Fig.3 SEM images of (a) PS and (b) SS

2.2 Preparation of specimens

The ratio of PS/SS was 0%-60% with 30% interval replacing cement by mass, and the content of TIPA was 0.03%, 0.06%, and 0.09% of cementitious materials, respectively. The mixture proportions of ternary cement pastes containing PS/SS and TIPA maintaining a water/cement ratio of 0.4 are shown in Table 2. The freshly mixture were cast into molds with side length of 40 mm, and put these in a curing room (20℃, ⩾ 90% RH). Demolded after 24 h and then cured further to 7, 28, and 60 d. The compressive strength of speci-

mens was tested, and the broken pieces were immersed in anhydrous ethanol 7 d to stop hydration. Then the samples were removed from anhydrous ethanol and dried in a vacuum oven at 50 ℃. A portion was ground to below 75 μm for XRD and TGA, and the remainder was used for MIP.

Table 2 Mixture proportions of the pastes

Notation	Mixture components/%				
	Cement	PS	SS	TIPA	Water
OPC	100	0	0	0	40
P30T0	70	30	0	0	40
P30T3	70	30	0	0.03	40
P30T6	70	30	0	0.06	40
P30T9	70	30	0	0.09	40
P60T0	40	60	0	0	40
P60T3	40	60	0	0.03	40
P60T6	40	60	0	0.06	40
P60T9	40	60	0	0.09	40
S30T0	70	0	30	0	40
S30T3	70	0	30	0.03	40
S30T6	70	0	30	0.06	40
S30T9	70	0	30	0.09	40
S60T0	40	0	60	0	40
S60T3	40	0	60	0.03	40
S60T6	40	0	60	0.06	40
S60T9	40	0	60	0.09	40

2.3 Methods

2.3.1 Compressive strength

Paste specimens with 40 mm side length were used to test the compressive strength at different curing ages. The final value was the average of three specimens.

2.3.2 Hydration heat

Isothermal Calorimeter with eight channels (TAM AIR, SETARAM, France) was used to test the change in heat flow during hydration of pastes over a 240 h period. 7 g pastes were continuously tested at 20 ℃.

2.3.3 Hydration products

The mineral phases of pastes were measured by XRD (D8 Advance, Germany, Cu-Kα radiation (λ = 0.154 nm), the step of 0.02°, 4 °/min from 5° to 70°). The hydration products of pastes were analyzed by TGA (STA449F3, Germany, room temperature −1 000 ℃, 10 ℃/min, nitrogen atmosphere).

2.3.4 Pore structure

The pore structure of hardened pastes was characterized by MIP (Poremaster GT-60, Kangta Instrument Company, USA, ≤ 210 MPa, 140°).

2.3.5 Solubility of PS and SS

The simulated pore solution was prepared with NaOH and KOH (Na^+ / K^+ = 1:1, pH = 13.0), and different content of TIPA (0 and 8 g/L) were added. PS/SS powders were immersed in the solution at a solid-liquid ratio of 1:20, and then left at 20 ℃ for 1, 3, 7, and 28 d. After centrifugation, the supernatant was taken, and Al and Fe contents of the supernatant was measured by ICP (Prodigy 7, USA). The solids were dried in a vacu-

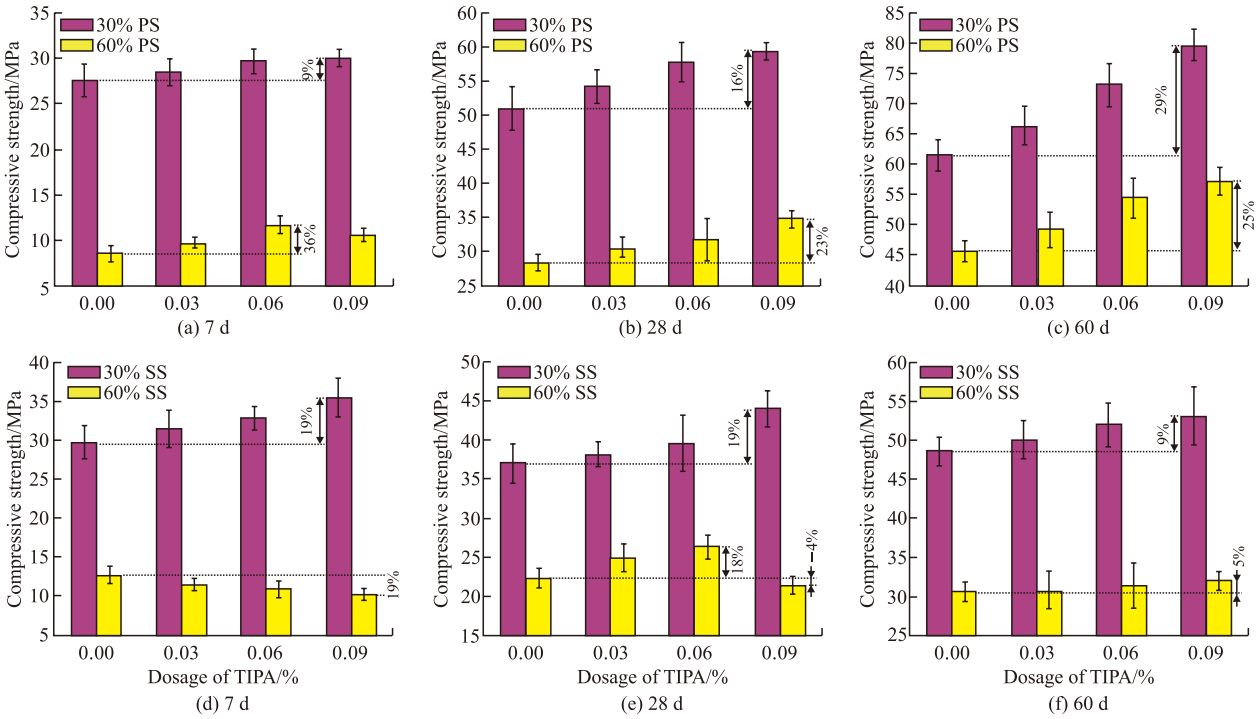

Fig.4 Compressive strength of hardened pastes

um oven at 50 ℃, and the micromorphology of PS and SS was characterized by SEM (QUANTA FEG 4500, FEI, 15 kV), respectively.

3 Results and discussion

3.1 Compressive strength

Fig.4 reveals the strength development of hardened specimens. Obviously, the addition of PS and SS reduces the compressive strength of pure cement (41.8 MPa at 7 d, 66.8 MPa at 28 d, and 68.6 MPa at 60 d), which decreases with increasing dosage, in addition the compressive strength increases with increasing curing time. At 7 d, specimens containing SS has a greater compressive strength than those containing PS under the same amount of SCMs. However, the rule is reversed at 28 and 60 d. For instance, the specimens with 30% PS, 60% PS, 30%SS and 60%SS exhibit a 34%, 80%, 29%, and 70% reduction in compressive strength at 7 d and 10%, 33%, 29%, and 56% reduction at 60 d compared to OPC, respectively. The results demonstrate the early activity of PS is inferior to that of SS and the later activity is superior to that of SS.

As can be observed from Fig.4, adding TIPA can enhance the compressive strength of specimens of cement-SCMs system, except for specimens containing 60% SS and TIPA at 7 d and those containing 60% SS and 0.09% TIPA at 28 d. For cement-PS system, that of specimens increases with increasing TIPA content, excluding specimens with 60% PS and 0.09% TIPA at 7 d. Moreover, specimens containing 30% PS excess the compressive strength of pure cement after 60 d whenever TIPA is present at a level greater than 0.06%. In comparison with specimens with 60% PS, the addition of 0.06% TIPA increases the compressive strength by 12% at 28 d and 19% at 60 d. For cement-SS system, the compressive strength increases with increasing TIPA content at 7, 28, and 60 d when SS content is 30%. However, when SS content is 60%, the compressive strength gradually decreases at 7 d, increases (TIPA content $\leqslant$ 0.06%) and then decreases (TIPA content > 0.06%) at 28 d, and progressively increases at 60 d as the amount of TIPA increases. For instance, compared with 60% SS specimens, adding 0.06% TIPA increases the compressive strength by 18% at 28 d and 3% at 60 d, respectively. Therefore, it can be concluded that the proper dosage of TIPA favours strength development in cement-PS system, and TIPA is detrimental to the early strength development in cement-SS system and favours the later strength development.

The above discussions show that incorporating TIPA can improve the strength of cementitious materials containing large amounts of PS and SS, and the specific details will be discussed in the following.

3.2 Hydration heat

Fig. 5 illustrates heat flow and cumulative heat of OPC, P60T0, P60T6, P60T9, S60T0, S60T6, and S60T9 within 240 h of paste hydration. From Figs.5(a), 5(c) and 5(e), the hydration process for all samples consists of five periods: pre-induction, induction, acceleration, deceleration and stable periods, and five different exothermic peaks can be observed, associated with I: C_3A hydration, II: C_3S hydration, III: SS hydration, IV: renewed ettringite (AFt) formation and V: AFt to monosulphate (AFm) conversion[33, 34]. In pre-induction period, the reaction peak (peak I) of C_3A hydration appears within a few minutes and AFt is generated, which makes it difficult to distinguish the exothermic rate of pastes[35]. Therefore, the pre-induction stage is not discussed.

In Fig.5(a), as for cement-SCMs system, 60wt% PS and SS extends the deadline for induction period by 5.20 and 1.82 h, respectively. The reaction peak (peak II) of C_3S hydration occurs during acceleration period, and the maximum heat flow of P60T0 (18.95 h, 1.19 mW/g) and S60T0 (12.26 h, 0.96 mW/g) are delayed and reduced in comparison to OPC (11.05 h, 2.86 mW/g). The main cause of the phenomenon is the diluting and retarding effects of PS and SS, which partially replaces cement resulting in a low clinker content in cementitious system[15,17]. In contrast, the dilution effect of SS is stronger than that of PS, and the retarding effect is weaker. In addition, S60T0 appears the exothermic peak (peak III) of SS hydration at approximate 33 h in deceleration period. In Fig. 5(b), compared to the 168 h cumulative heat of OPC (287.95 J/g), that of P60T0 (143.85 J/g) and S60T0 (154.71 J/g) is reduced by 50.04% and 46.27%, respectively, both lower than 60wt% replacement rate. This is attributed to the dilution effect of PS and SS increasing the effective water-cement ratio, and the nucleation effect providing nucleation sites, which accelerate cement hydration and produce more heat[36].

According to Figs.5(c) and 5(e), adding TIPA to cement-SCMs system causes a significantly change in hydration process, and the influences of TIPA on cement-PS system and cement-SS system are discussed separately below:

(1) Cement-PS system

In induction period, the heat flow of P60T0 is

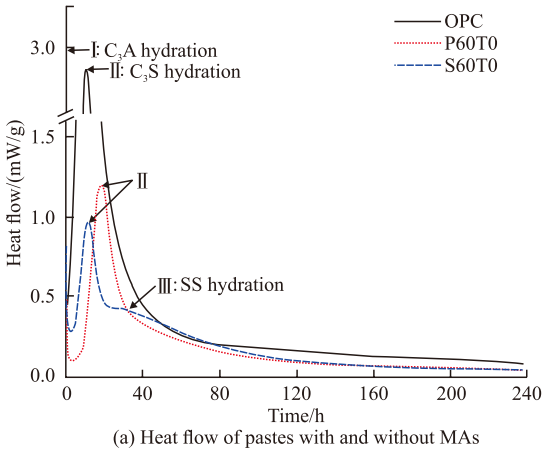

(a) Heat flow of pastes with and without MAs

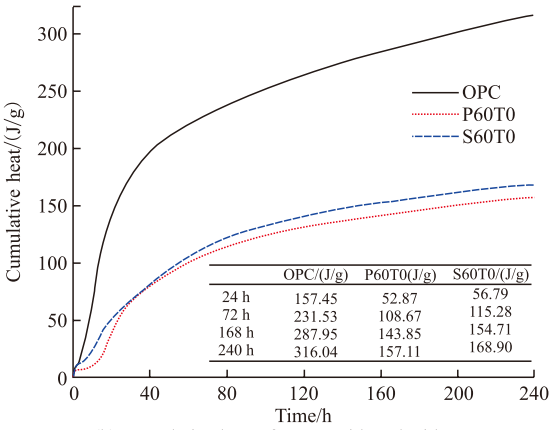

(b) Cumulative heat of pastes with and without MAs

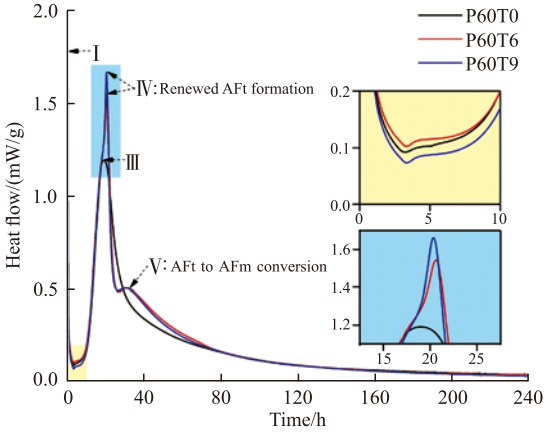

(c) Heat flow of cement-PS system with and without TIPA

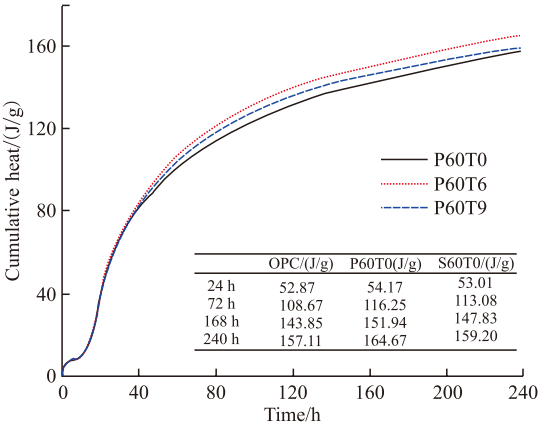

(d) Cumulative heat of cement-PS system with and without TIPA

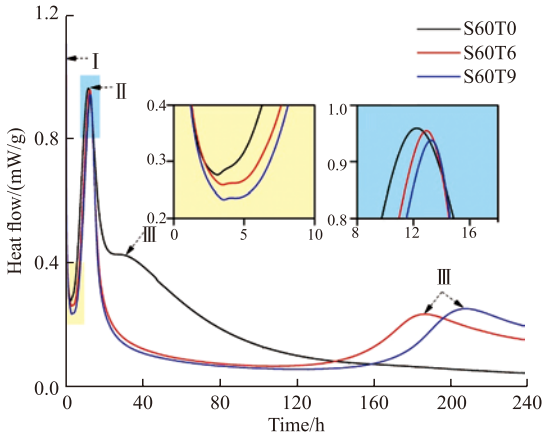

(e) Heat flow of cement-SS system with and without TIPA

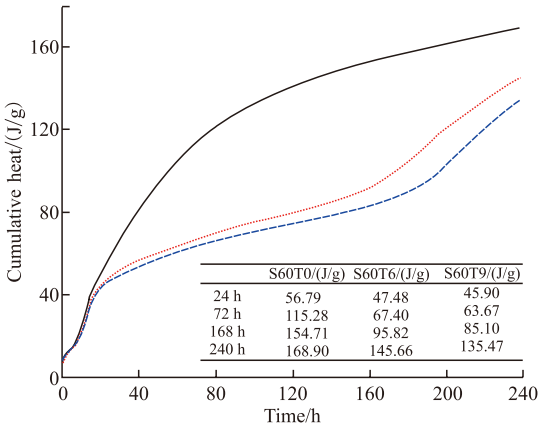

(f) Cumulative heat of cement-SS system with and without TIPA

Fig. 5 Hydration heat of different pastes during 240 h

lower than that of P60T6, and higher than that of P60T9. In acceleration period, the peak IV appears in P60T6 at 20.63 h with 1.54 mW/g and P60T9 at 20.36 h with 1.66 mW/g, demonstrating that TIPA facilitates secondary AFt formation[37]. This causes that depletion of sulphate in the pore solution[6]. Therefore, the exothermic peak (peak V) of reaction between AFt and C_3A to form AFm appears at around 31 h in deceleration period[38]. Then hydration reaction goes to stable period. In Fig.5(d), the cumulative heat of P60T6 and P60T9 before 240 h hydration is higher than that of P60T0 with a decreasing trend according to P60T6 > P60T9 > P60T0, which is in agreement with the strength pattern of specimens at 7 d. The results demonstrate that TIPA promotes the hydration of cement-PS system, and a suitable dosage of TIPA accelerates it.

(2) Cement-SS system

In contrast to S60T0, TIPA reduces the flow heat during induction period and prolongs it. In acceleration period, the maximum heat flow of S60T6 and S60T9

is 0.95 mW/g at 12.92 h and 0.94 mW/g at 13.26 h, respectively. S60T6 and S60T9 do not exhibit peak III during deceleration period, but a broad peak about SS hydration occurs during stable period at approximately 186 h and 207 h, respectively. It is worth from Fig.5(f) that the cumulative heat of S60T6 and S60T9 is always lower than that of S60T0 before 240 h with a decreasing trend in order: S60T0 > P60T6 > P60T9, which is comsistent with the strength pattern of specimens at 7 d. However, that of S60T6 and S60T9 increases rapidly at about 130 h and 150 h, respectively, and narrows the gap with that of S60T0. This demonstrates that TIPA inhibits the early hydration of cement-SS system.

3.3 Hydrates analysis

3.3.1 XRD analysis

Fig.6 presents XRD patterns of samples, revealing that unhydrated alite (C_3S) and belite (C_2S), hydrated portlandite (CH), and carbonated CH forming calcite ($CaCO_3$) are present in each curing age of each sample. The intensity of unhydrated peaks decrease and the intensity of hydrated peaks increase with longer curing. In contrast to OPC, some different hydration product peaks can be observed owing to the addition of other materials.

For cement-PS-TIPA system, at 7 d (Fig.6(a)), the hydrated peaks of ettringite (AFt, generated by the reaction of C_3A and gypsum) and hemicarbonate (Hc, formed by the reaction of C_3A and $CaCO_3$) occur in P60T0[39]. By comparison, the peaks of AFt disappear, and the peaks of monosulphate (Ms, AFm, generated by the reaction of C_3A and AFt) and monocarbonate (Mc, generated by the reaction of C_3A and $CaCO_3$) appear in P60T6[38]. This demonstrates that TIPA facilitated the transition from AFt to AFm[40], and also proves the law of Fig.5(c). It is worth noting that C_4AF peak cannot be observed in P60T6, which verifies the promotion of C_4AF hydration by TIPA. C_4AF and C_3A of mineral phase of clinker have similar hydration reactions and products, reacting with gypsum in the presence of gypsum to generate AFt, and reacting with AFt on the depletion of gypsum to form AFm[41,42]. TIPA accelerates the amount of dissolved Al and Fe, thus promoting the production of renewed AFt (produced by C_4AF), resulting in the depletion of gypsum and the transformation from AFt to AFm. At 60 d (Fig.6(b)), Ht appears in P60T0 owing to the liberation of MgO from PS[43]. Ms disappears and Hc occurs in P60T6.

For cement-SS-TIPA system, the intensity of Fe-monocarbonate (Fe-Mc) and Mc peaks in S60T6 are higher than that in S60T0 at 7 d (Fig.6(a)), while the intensity of Mc peak is lower than that in S60T0 at 60 d (Fig.6 (b)). C_4AF appears in P60T6 at 7 d and disappears at 60 d. The mineral phases magnetite (Fe_3O_4) and RO phase are also observed in S60T0 and S60T6. Based on previous research[44], the Fe-Mc diffraction peaks were detected in the presence of calcite and rich iron. In this experiment, calcite present in SS and rich iron ions generated by TIPA to promote SS dissolution, thus Fe-Mc is generated in specimens with high SS content.

3.3.2 TG-DTG analysis

Fig.7 gives TG-DTG analysis of samples. The endothermic peaks in different temperature ranges on the DTG curves correspond to the dehydration or decomposition of different substances, specifically peak around 100 ℃ refers to the decomposition of C-S-H or AFt, peak around 150 ℃ relates to the decomposition of carboaluminate/Fe-Mc or AFm phase, peak around

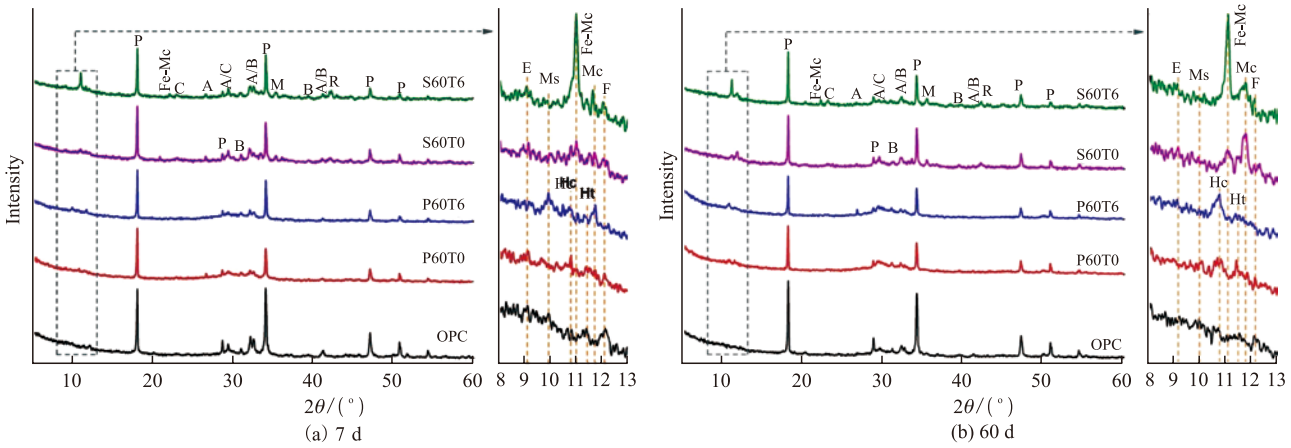

Fig.6 XRD patterns of samples. (E: ettringite, Ms: monosulphate, Hc: hemicarbonate, Ht: hydrotalcite, Mc:monocarbonate, Fe-Mc: Fe-monocarbonate,P: portlandite, C: calcite, A: alite, B: belite, F: ferrite, M: magnetite, R: RO phase)

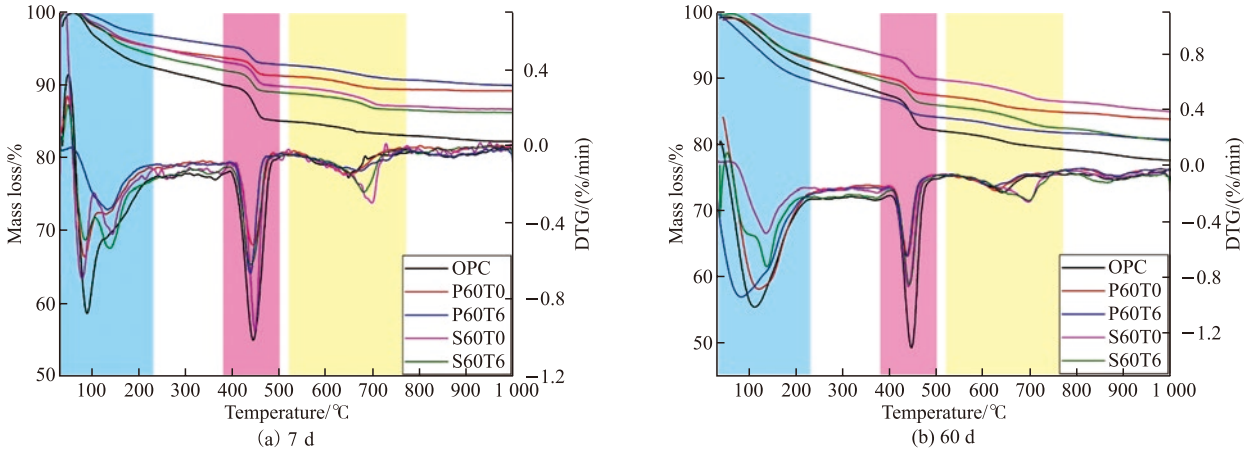

Fig.7 TGA curves of samples at (a) 7 d and (b) 60 d

440℃ (380-500 ℃) belongs to the dehydration of CH, and peak around 650 ℃ (520-770 ℃) attributes to the decomposition of less crystalline $CaCO_3$ formed in the course of sample preparation due to CH carbonation[44-48]. Mass loss in different temperature ranges and CH content calculated in light of TG results and Eq.(1) are listed in Table 3[48].

$$CH_{content}=m_{3580\text{-}500℃}\times\frac{74}{18}+m_{520\text{-}770℃}\times\frac{74}{44} \quad (1)$$

For cement-SCMs system, the mass loss at less than 230 ℃ is 4.86% and 4.82% for P60T0 and S60T0 respectively at 7 d, both lower than 7.64% for OPC. Furthermore, the CH content of P60T0 and S60T0 is also less than that of OPC. When curing for 60 d, there is the same rule. This is mainly because PS and SS are less reactive than cement.

Table 3 Mass loss of pastes/wt%

Sample	Less than 230 ℃	380-500 ℃	520-770 ℃	CH content
		7 d		
OPC	7.64	4.93	1.92	23.48
P60T0	4.86	2.48	1.79	13.21
P60T6	3.20	2.56	2.02	13.91
S60T0	4.82	3.34	2.66	18.20
S60T6	5.89	3.04	2.29	16.35
		60 d		
OPC	8.73	5.71	2.69	28.00
P60T0	7.35	2.89	2.41	15.95
P60T6	10.48	2.90	2.23	15.66
S60T0	3.98	3.73	3.23	20.75
S60T6	7.13	3.77	3.32	21.09

When 0.06% TIPA is added to the cement-PS and cement-SS systems, a clear endothermic peak of carboaluminate/Fe-Mc can be observed, indicating that TIPA is helpful for forming production of carboaluminate/Fe-Mc. The CH content of P60T6 is higher than that of P60T0 in the early stage, but lower than that of P60T0 in the later stage. For sample containing SS, the rule is reversed when TIPA is added. This is because PS has hydration and pozzolanic activities, which will generate C-S-H in the presence of CH and consume CH to generate C-S-H[49,50]. SS contains the mineral phase of clinker, which will hydrate to form CH. This further verifies TIPA promotes hydration of PS and SS.

3.4 MIP analysis

The pore structure of hardened pastes is intimately associated with strength, therefore those of OPC, P60T0, P60T6, S60T0, and S60T6 cured for 60 d were measured using MIP. Fig.8(a) gives the cumulative porosity of samples. Compared to OPC with a porosity of 0.0917 mL/g, the porosity of P60T0 and S60T0 increases by 20.39% and 110.80%, respectively. For blended pastes with 0.06% TIPA, the porosity of P60T6 decreases by 38.59% in comparison with that of P60T0, and that of S60T6 decreases by 6.10% in comparison with that of S60T0. These results are in accordance with the rules of strength (shown in Fig.4(c)) in order: OPC > P60T0 > S60T0, P60T6 > P60T0, and S60T6 > S60T0.

Fig.8(b) gives the pore size distribution of pastes. Most probable aperture (MPA), the highest peak corresponding to the pore size in graph, for OPC, P60T0 and S60T0 are 40.87, 8.12, and 70.25 nm respectively, indicating that PS enhances the amount of small pores and refines pore structure, and SS reduces that and deteriorates pore structure[23,51]. MPA of P60T6 is less than 7.08 nm, below that of P60T0. MPA of S60T0 is 70.91 nm, which is approximately equal to that of S60T0. To im-

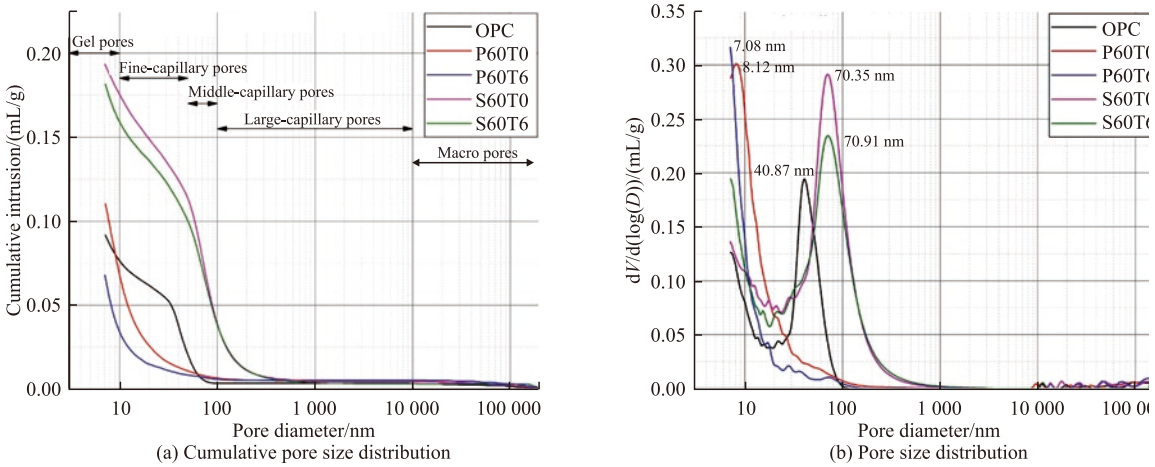

Fig.8 (a) Cumulative porosity and (b) pore size distribution of specimens at 60 d

prove understanding of the influence of TIPA on pastes mixed with PS or SS, the pores are classified according to as gel, fine-capillary, middle-capillary, large-capillary and macro pores, as in Fig.8(a)[51,52].

The pore volume proportion of pastes was calculated and is shown in Fig.9. In comparison with OPC, 60% PS increases the volume fraction of gel pores and decreases that of fine-capillary pores, while 60% SS reduces that of gel and fine-capillary pores. It can be deduced that fine-capillary pores are transformed into gel pores owning to continuous hydration in cement-PS system, while a large amount of SS reduces hydration products in cement-SS system.

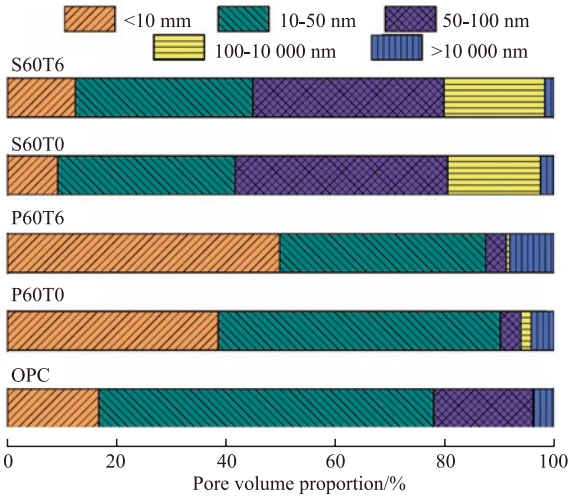

Fig.9 Pore volume proportion of pastes at 60 d

When adding 0.06% TIPA into cement-SCMs system, pore structure of pastes is refined. The volume fraction of gel pores in P60T6 is increased from 38.64% to 49.84%, and that of fine-capillary pores is decreased from 51.47% to 37.60% compared to P60T0. That of gel and fine-capillary pores in S60T6 is increased from 9.33% to 12.48% and from 32.33% to 32.44% respectively, compared with S60T0. According to the Ref.[52], pore sizes over 50 nm are not conducive to strength development. The results prove that TIPA accelerates the hydration of cement-SCMs system, and further refines the microstructure of pastes. These reaffirm the strength results.

3.5 Dissolution of PS and SS

To further explore the impact of TIPA on PS and SS, dissolved Al and Fe in PS and SS were measured in stimulated pore solutions, and the results are presented in Fig.10 and Fig.11, respectively. In Fig. 10, TIPA strongly increases dissolved amounts of Al and Fe ions from PS. Compared with the control group (without TIPA), Al ion concentration in the solution with TIPA is 1.05, 2.05, 2.68, and 6.26 times higher at 1, 3, 7, and 28 d, respectively. However, there is only a small amount of Fe ions in the control group. When TIPA is added, the amount of dissolved Fe ions steadily increases over 3 d, and then remains stable.

As shown in Fig. 11, without TIPA, there is no significant amount of dissolved Al and Fe ions in SS. With TIPA the dissolution concentration of Al ions rapidly reaches a maximum value, and then decreases continuously indicating that Al ions participate in the hydration reaction. Contrary to Al ions, the dissolution concentration of Fe ions reaches to 352.39 mg/L at 1 d, and then continuous increases to 831.78 mg/L at 28 d, while without TIPA the dissolution concentration of Fe ions is 1.97 mg/L at 1 d and 2.06 mg/L at 28 d.

Without TIPA, Al and Fe ions in PS and SS are not easily dissolved into the pore solution during hydration. TIPA accelerates the dissolution of Al and Fe ions in PS and SS, facilitates the erosion of surface of particles. Therefore, TIPA has a facilitating effect on pozzolanic and hydration reactivities of PS and SS.

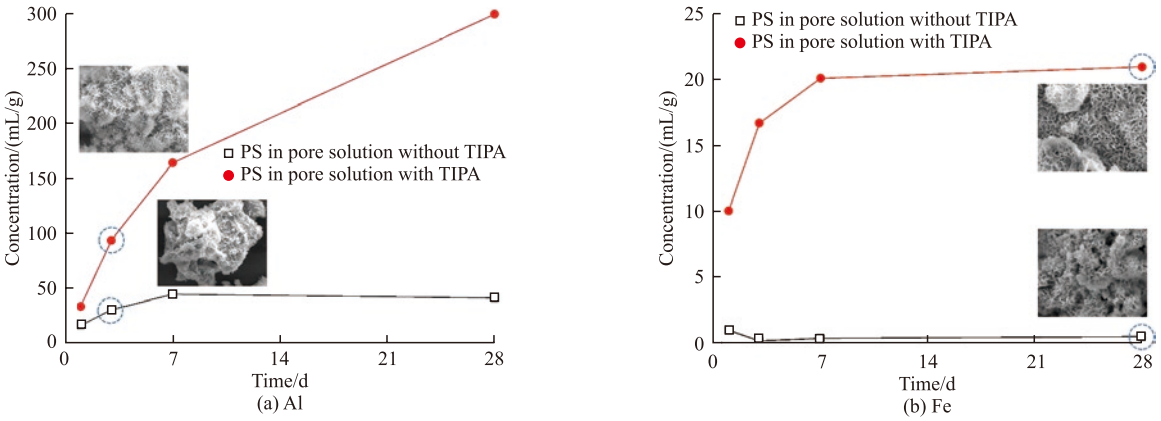

Fig.10 Ion dissolution of (a) Al and (b) Fe from PS

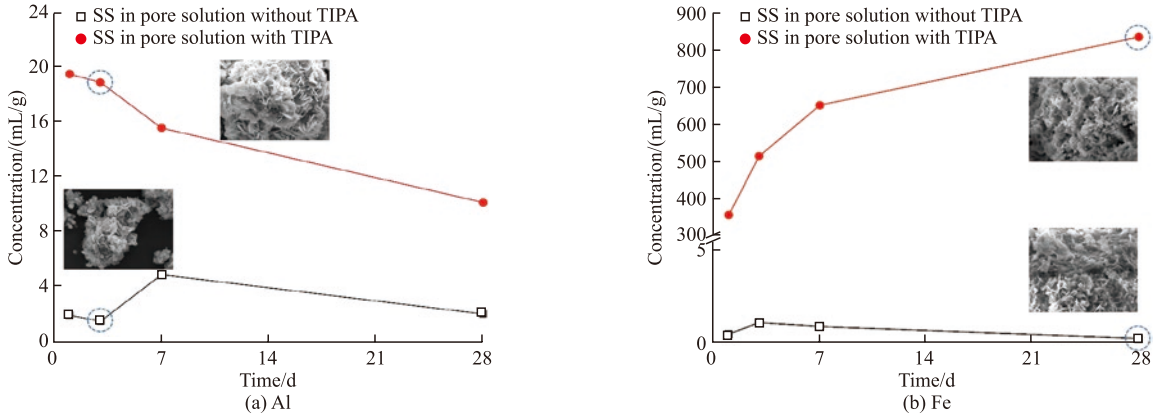

Fig.11 Ion dissolution of (a) Al and (b) Fe from SS

3.6 Reaction mechanism

In light of these results, the addition of TIPA has a significant contributor on the strength of high PS content pastes, but for high SS content pastes, the early strength is inhibited and the late is promoted. The hydration of cement-PS system and cement-SS system by TIPA is different, mainly because the chemical compositions of PS and SS are distinct, and the dissolution amount of ions promoted by TIPA in PS and SS is very different, which results in inconsistent hydration products and hydration mechanisms.

At the initial hydration stage, cement particles dissolve in water making the aqueous solution immediately become a solution containing multiple ions (such as Ca^{2+}, $Al(OH)_4^-$, SO_4^{2-}, OH^-, *etc*). By now, AFt generation reaction occurs, as shown in Eq. (2)[44]. Meanwhile, P_2O_5 and F in PS[17,53-55] and MgO, MnO and P_2O_5 in SS[26,56,57] inhibit cement hydration extending the induction period (as in Fig.5(a)). Then the hydration enters the acceleration period with C_3S hydrating to form C-S-H gels and CH (as in Eq.(3)). During the deceleration period, reactions between and generated by SS hydrolysis and Ca^{2+}, and OH^- in the paste generate small amounts of C-S-H gels and AFt, as in Eq.(4) and Eq.(2)[58]. Finally, the hydration enters the stable period. At the late hydration stage, the pozzolanic reaction of PS occurs, as in Eq.(5), and hydration reaction Eq.(2) and Eq.(4) continue to occur. Due to the higher activity of PS than SS, specimens with high PS content has a higher late strength than those with the same content of SS:

$$6Ca^{2+}+2Al(OH)_4^-+3SO_4^{2-}+4OH^-+26H_2O\rightarrow Ca_6Al_2(SO_4)_3(OH)_{12}\cdot 26H_2O(AFt) \quad (2)$$

$$C_3S+nH_2O\rightarrow C\text{-}S\text{-}H+(3\text{-}x)CH \quad (3)$$

$$2Ca^{2+}+SO_4^{4-}+2H_2O\rightarrow C\text{-}S\text{-}H+Ca^2+2OH^- \quad (4)$$

$$\text{Amorphus } SiO_2(PS)+CH\rightarrow C\text{-}S\text{-}H \quad (5)$$

There is general belief that TIPA accelerates the hydration of cement by forming Fe-TIPA chelates to promote the dissolution of mineral phases[38,47]. For improve the strength of specimens with high SCMs content, TIPA is introduced. At the early hydration stage, According to Section 3.5, TIPA promotes the dissolution of Al ions in PS (as in Fig.10(a)), which leads

to the accelerated consumption of SO_4^{2-} in cement-PS system and the generation of secondary AFt (as in Eq.(2)) in the acceleration period. The premature depletion of results in AFm generation during the deceleration period, as in Eq.(6). The CO_3^{2-} dissolved in raw materials also react with Ca^{2+} and $Al(OH)_4^-$ to form Mc and Hc, as in Eq.(7) and Eq.(8)[38, 59]. In cement-SS system, TIPA promotes the substantial leaching of Fe ions in SS (in Fig.11(b)), thus facilitating the reaction of $Fe(OH)_4^-$ with Ca^{2+}, CO_3^{2-} and OH^- to form Fe-Mc, as in Eq.(9)[44]. Combined with Fig.5(e) and Fig.6(a), it can be analyzed that Fe-Mc precipitates on the surface of SS particles and hinders SS hydration[44]. At the late hydration stage, TIPA continuous to promotes the ions dissolution in cementitious system, accelerating the hydration of cement, PS and SS. With the interpenetration and lapping of hydration products, the specimens gradually become compact, which is beneficial to the strength improvement.

$$4Ca^{2+}+2Al(OH)_4^-+SO_4^{2-}+4OH^-+6H_2O\rightarrow Ca_4Al_2(SO_4)(OH)_{12}\cdot 6H_2O(AFm) \quad (6)$$

$$4Ca^{2+}+2Al(OH)_4^-+CO_3^{2-}+4OH^-+5H_2O\rightarrow Ca_4Al_2(CO_3)(OH)_{12}\cdot 5H_2O(Mc) \quad (7)$$

$$4Ca^{2+}+2Al(OH)_4^-+0.5CO_3^{2-}+5OH^-+5.5H_2O\rightarrow Ca_4Al_2(CO_3)_{0.5}(OH)_{12}\cdot 6H_2O(Hc) \quad (8)$$

$$4Ca^{2+}+2Fe(OH)_4^-+CO_3^{2-}+4OH^-+6H_2O\rightarrow Ca_4Fe_2(CO_3)(OH)_{12}\cdot 6H_2O(Fe\text{-}Mc) \quad (9)$$

3.7 Carbon emission assessment

To assess the environment benefits of different cementitious materials, CO_2 emissions is calculated. Table 4 lists CO_2 emissions of raw materials. CO_2 emissions of cement is 840 kg/t[60, 61]. PS and SS are industrial wastes, and therefore CO_2 emissions owing to grinding process are solely considered. CO_2 emissions of PS and SS are 118 and 157 kg/t, respectively. Besides, that of TIPA is 418 kg/t[62].

Table 4 CO_2 emissions of raw materials/(kg/t)

Material	Cement	PS	SS	TIPA
CO_2 emission	840	118	157	418

Fig.12 illustrates CO_2 emissions of different cementitious material. CO_2 emissions for single cement is 840.0 kg/t, and that for blends containing 60% PS and SS are 406.8 and 430.2 kg/t, respectively. Further addition of TIPA has little effect on CO_2 emissions of the blends. Therefore, it can be calculated that CO_2 emissions of 60% PS or 60% SS blends with TIPA have a reduction of 51.54% or 48.75%, compared to that of single cement. It has been proved that the use of PS and SS can greatly reduce CO_2 emissions of cementitious materials.

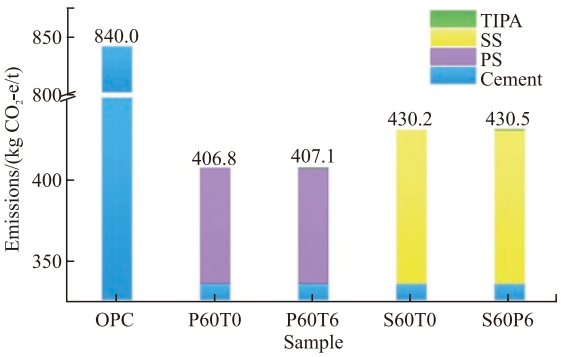

Fig.12 CO_2 emissions of different cementitious materials

4 Conclusions

In this study, low-carbon cementitious materials were prepared by incorporating high content of PS and SS, and the effect of TIPA on hydration process of cement-PS and cement-SS systems were studied. The conclusions are shown as follows:

a) The replacement of cement with 60% PS or 60% SS significantly decreased the compressive strength of specimens, and a reduction of 57% or 67% at 28 d. Fortunately, the incorporation of TIPA compensated for the strength deficiencies caused by the high content of PS and SS. The compressive strength of cement containing 60% PS or 60% SS was enhanced by 12% or 18% at 28 d. However, TIPA is unfavorable for early strength of cement with 60% SS.

b) AS for cement-PS-TIPA system, in the early stage, TIPA accelerated the dissolution of Al ions in PS, and the formation of carboaluminate hydrate was facilitated, which could induce the hydration; and in the later stage, the pozzolanic reaction of PS was promoted under the continuous solubilization effect of TIPA, and more C-S-H gels were generated, resulting in a refinement of pore structure of specimens and a reduction in MPA from 8.12 nm to less than 7.08 nm.

c) As for cement-SS-TIPA system, in the early stage, TIPA promoted the dissolution of Fe ions in SS, and the formation of Fe-Mc, which is precipitated on the surface of SS, resulting in the postponement of hydration, especially for the high SS content; and in the later stage, TIPA promoted the hydraulic reactions of SS due to its solubilization effect, and more CH were

generated, leading to lower porosity from 0.1933 mL/g to 0.1815 mL/g.

d) Compared with Portland cement, the carbon emissions of cement-PS-TIPA and cement-SS-TIPA was reduced by 52% and 49%, respectively. Thereby, PS and SS could be expected to be used to prepare low-carbon cementitious materials when used in conjunction with TIPA.

Conflict of interest

All authors declare that there are no competing interests.

References

[1] Aslam B, Hu J, Hafeez M, *et al*. Applying Environmental Kuznets Curve Framework to Assess the Nexus of Industry, Globalization, and CO_2 Emission[J]. *Environmental Technology & Innovation*, 2021, 21: 101 377

[2] Ren F-r, Tian Z, Liu J, *et al*. Analysis of CO_2 Emission Reduction Contribution and Efficiency of China's Solar Photovoltaic Industry: Based on Input-Output Perspective[J]. *Energy*, 2020, 199: 117 493

[3] Benhelal E, Shamsaei E, Rashid MI. Challenges against CO_2 Abatement Strategies in Cement Industry: A Review[J]. *J. Environ. Sci. (China)*, 2021, 104: 84-101

[4] Ofosu-Adarkwa J, Xie N, Javed SA. Forecasting CO_2 Emissions of China's Cement Industry Using a Hybrid Verhulst-Gm(1,N) Model and Emissions' Technical Conversion[J]. *Renewable and Sustainable Energy Reviews*, 2020, 130: 109 945

[5] Belbute JM, Pereira AM. Reference Forecasts for CO_2 Emissions from Fossil-Fuel Combustion and Cement Production in Portugal[J]. *Energy Policy*, 2020, 144: 111 642

[6] Zhang MH, Islam J. Use of Nano-Silica to Reduce Setting Time and Increase Early Strength of Concretes with High Volumes of Fly Ash or Slag[J]. *Construction and Building Materials*, 2012, 29: 573-580

[7] Özbay E, Erdemir M, Durmuş Hİ. Utilization and Efficiency of Ground Granulated Blast Furnace Slag on Concrete Properties – a Review[J]. *Construction and Building Materials*, 2016, 105: 423-434

[8] Du C, Tan H, Jian S, *et al*. Compressive Strength and Hydration Process of Sodium Carbonate-Activated Superfine Slag/Marble Powder Binders[J]. *Journal of Building Engineering*, 2021, 43: 103 121

[9] Shen W, Liu Y, Yan B, *et al*. Cement Industry of China: Driving Force, Environment Impact and Sustainable Development[J]. *Renewable and Sustainable Energy Reviews*, 2017, 75: 618-628

[10] Bhagath Singh GVP, Subramaniam KVL. Production and Characterization of Low-Energy Portland Composite Cement from Post-Industrial Waste[J]. *Journal of Cleaner Production*, 2019, 239: 118 024

[11] Lothenbach B, Scrivener K, Hooton RD. Supplementary Cementitious Materials[J]. *Cement and Concrete Research*, 2011, 41(12): 1 244-1 256

[12] Yang J, Huang J, He X, *et al*. Shrinkage Properties and Microstructure of High Volume Ultrafine Phosphorous Slag Blended Cement Mortars with Superabsorbent Polymer[J]. *Journal of Building Engineering*, 2020, 29: 101 121

[13] Martins ACP, Franco de Carvalho JM, Costa LCB, *et al*. Steel Slags in Cement-Based Composites: An Ultimate Review on Characterization, Applications and Performance[J]. *Construction and Building Materials*, 2021, 291: 123 265

[14] Peng Y, Zhang J, Liu J, *et al*. Properties and Microstructure of Reactive Powder Concrete Having a High Content of Phosphorous Slag Powder and Silica Fume[J]. *Construction and Building Materials*, 2015, 101: 482-487

[15] Zhuang S, Wang Q. Inhibition Mechanisms of Steel Slag on the Early-Age Hydration of Cement[J]. *Cement and Concrete Research*, 2021, 140: 106 283

[16] Yang Q, Li C, Ren Q, *et al*. Properties and Microstructure of Co_2 Activated Binder Produced by Recycling Phosphorous Slag[J]. *Construction and Building Materials*, 2021, 282: 122 698

[17] Wang L, Guo F, Lin Y, *et al*. Comparison between the Effects of Phosphorous Slag and Fly Ash on the C-S-H Structure, Long-Term Hydration Heat and Volume Deformation of Cement-Based Materials[J]. *Construction and Building Materials*, 2020, 250: 118 807

[18] Chen L, Wang H, Zheng K, *et al*. The Mechanism of Basic Oxygen Furnace Steel Slag Retarding Early-Age Hydration of Portland Cement and Mitigating Approach Towards Higher Utilization Rate[J]. *Journal of Cleaner Production*, 2022, 362: 132 493

[19] Li J, Yu Q, Wei J, *et al*. Structural Characteristics and Hydration Kinetics of Modified Steel Slag[J]. *Cement and Concrete Research*, 2011, 41(3): 324-329

[20] Muhmood L, Vitta S, Venkateswaran D. Cementitious and Pozzolanic Behavior of Electric Arc Furnace Steel Slags[J]. *Cement and Concrete Research*, 2009, 39(2): 102-109

[21] Zhang N, Wu L, Liu X, *et al*. Structural Characteristics and Cementitious Behavior of Basic Oxygen Furnace Slag Mud and Electric Arc Furnace Slag[J]. *Construction and Building Materials*, 2019, 219: 11-18

[22] Guo J, Bao Y, Wang M. Steel Slag in China: Treatment, Recycling, and Management[J]. *Waste Management*, 2018, 78: 318-330

[23] Zhang T, Ma B, Wu S, *et al*. Mechanical Properties and Hydration Process of Steel Slag-Cement Binder Containing Nano-SiO_2[J]. *Construction and Building Materials*, 2022, 314: 125 660

[24] Kansal CM, Goyal R. Effect of Nano Silica, Silica Fume and Steel Slag on Concrete Properties[J]. *Materials Today: Proceedings*, 2021, 59: 4 535-4 540

[25] Huo B, Li B, Chen C, *et al*. Surface Etching and Early Age Hydration Mechanisms of Steel Slag Powder with Formic Acid[J]. *Construction and Building Materials*, 2021, 280: 122 500

[26] You N, Li B, Cao R, *et al*. The Influence of Steel Slag and Ferronickel Slag on the Properties of Alkali-Activated Slag Mortar[J]. *Construction and Building Materials*, 2019, 227: 116 614

[27] Xie F, Liu Z, Zhang D, *et al*. The Effect of NaOH Content on Rheological Properties, Microstructures and Interfacial Characteristic of Alkali Activated Phosphorus Slag Fresh Pastes[J]. *Construction and Building Materials*, 2020, 252: 119 132

[28] Kong Y, Wang P, Liu S. Microwave Pre-Curing of Portland Cement-Steel Slag Powder Composite for Its Hydration Properties[J]. *Construction and Building Materials*, 2018, 189: 1 093-1 104

[29] Han F, Zhang Z, Wang D, *et al*. Hydration Heat Evolution and Kinetics of Blended Cement Containing Steel Slag at Different Temperatures[J]. *Thermochimica Acta*, 2015, 605: 43-51

[30] Huang H, Shen XD. Statistical Study of Cement Additives with and without Chloride on Performance Modification of Portland Cement[J]. *Progress in Natural Science: Materials International*, 2011, 21(3): 246-253

[31] Tian L, Dai S, Yao X, *et al*. Effect of Nucleation Seeding and Triisopropanolamine on the Compressive Strength, Chloride Binding Capacity and Microstructure of Cement Paste[J]. *Journal of Building Engineering*, 2022, 52: 104 382

[32] Gartner E, Myers D. Influence of Tertiary Alkanolamines on Portland Cement Hydration[J]. *Journal of the American Ceramic Society*, 1993, 76(6): 1 521-1 530

[33] Huang H, Li XR, Shen XD. Hydration of Ternary Cement in the Presence of Triisopropanolamine[J]. *Construction and Building Materials*, 2016, 111: 513-521

[34] Bullard JW, Jennings HM, Livingston RA, *et al*. Mechanisms of Cement Hydration[J]. *Cement and Concrete Research*, 2011, 41(12): 1 208-1 223

[35] Hu X, Shi C, Shi Z, *et al*. Early Age Shrinkage and Heat of Hydration of Cement-Fly Ash-Slag Ternary Blends[J]. *Construction and Building Materials*, 2017, 153: 857-865

[36] Zhang T, Ma B, Jiang D, *et al*. Comparative Research on the Effect of Various Mineral Admixtures on the Early Hydration Process of Cement[J]. *Construction and Building Materials*, 2021, 301: 124 372

[37] Buil M, Paillère AM, Roussel B. High Strength Mortars Containing Condensed Silica Fume[J]. *Cement and Concrete Research*, 1984, 14(5): 693-704

[38] Wang J, Ma BG, Tan HB, *et al*. Hydration and Mechanical Properties of Cement-Marble Powder System Incorporating Triisopropanolamine[J]. *Construction and Building Materials*, 2021, 266: 121 068

[39] Ma B, Wang J, Tan H, *et al*. Utilization of Waste Marble Powder in Cement-Based Materials by Incorporating Nano Silica[J]. *Construction and Building Materials*, 2019, 211: 139-149

[40] Cheung J, Jeknavorian A, Roberts L, *et al*. Impact of Admixtures on the Hydration Kinetics of Portland Cement[J]. *Cement and Concrete Research*, 2011, 41(12): 1 289-1 309

[41] Cuesta A, Santacruz I, Sanfélix SG, *et al*. Hydration of C_4af in the Presence of Other Phases: A Synchrotron X-Ray Powder Diffraction Study[J]. *Construction and Building Materials*, 2015, 101: 818-827

[42] Fukuhara M, Goto S, Asaga K, *et al*. Mechanisms and Kinetics of C_4AF Hydration with Gypsum[J]. *Cement and Concrete Research*, 1981, 11(3): 407-414

[43] Haha MB, Lothenbach B, Le Saout G, *et al*. Influence of Slag Chemistry on the Hydration of Alkali-Activated Blast-Furnace Slag - Part I: Effect of MgO[J]. *Cement and Concrete Research*, 2011, 41(9): 955-963

[44] Dilnesa B Z, Lothenbach B, Le Saout G, *et al*. Iron in Carbonate Containing Afm Phases[J]. *Cement and Concrete Research*, 2011, 41(3): 311-323

[45] Liu M, Tan H, He X. Effects of Nano-SiO_2 on Early Strength and Microstructure of Steam-Cured High Volume Fly Ash Cement System[J]. *Construction and Building Materials*, 2019, 194: 350-359

[46] Zhang B, Tan H, Shen W, *et al*. Nano-Silica and Silica Fume Modified Cement Mortar Used as Surface Protection Material to Enhance the Impermeability[J]. *Cement and Concrete Composites*, 2018, 92: 7-17

[47] Huang H, Shen XD. Interaction Effect of Triisopropanolamine and Glucose on the Hydration of Portland Cement[J]. *Construction and Building Materials*, 2014, 65: 360-366

[48] De Weerdt K, Haha MB, Le Saout G, *et al*. Hydration Mechanisms of Ternary Portland Cements Containing Limestone Powder and Fly Ash[J]. *Cement and Concrete Research*, 2011, 41(3): 279-291

[49] Almeida F C R, Klemm A J. Efficiency of Internal Curing by Superabsorbent Polymers (SAP) in PC-GGBS Mortars[J]. *Cement and Concrete Composites*, 2018, 88: 41-51

[50] Zou F, Tan H, He X, *et al*. Effect of Triisopropanolamine on Compressive Strength and Hydration of Steaming-Cured Cement-Fly Ash Paste[J]. *Construction and Building Materials*, 2018, 192: 836-845

[51] Xu Z, Gao J, Zhao Y, *et al*. Promoting Utilization Rate of Ground Granulated Blast Furnace Slag (GGBS): Incorporation of Nanosilica to Improve the Properties of Blended Cement Containing High Volume GGBS[J]. *Journal of Cleaner Production*, 2022, 332: 130 096

[52] Zhang J, Tan H, Cai L, *et al*. Ultra-Fine Slag Activated by Sodium Carbonate at Ambient Temperature[J]. *Construction and Building Materials*, 2020, 264: 120 695

[53] Xie F, Liu Z, Zhang D, *et al*. Understanding the Acting Mechanism of NaOH Adjusting the Transformation of Viscoelastic Properties of Alkali Activated Phosphorus Slag[J]. *Construction and Building Materials*, 2020, 257: 119 488

[54] Chen X, Zeng L, Fang K. Anti-Crack Performance of Phosphorus Slag Concrete[J]. *Wuhan University Journal of Natural Sciences*, 2009, 14(1): 80-86

[55] Allahverdi A, Pilehvar S, Mahinroosta M. Influence of Curing Conditions on the Mechanical and Physical Properties of Chemically-Activated Phosphorous Slag Cement[J]. *Powder Technology*, 2016, 288: 132-139

[56] Péra J, Ambroise J, Chabannet M. Properties of Blast-Furnace Slags Containing High Amounts of Manganese[J]. *Cement and Concrete Research*, 1999, 29(2): 171-177

[57] Liu Z, Cui X, Tang M. Hydration and Setting Time of MgO-Type Expansive Cement[J]. *Cement and Concrete Research*, 1992, 22(1): 1-5

[58] Chen P, Ma B, Tan H, *et al*. Improving the Mechanical Property and Water Resistance of B-Hemihydrate Phosphogypsum by Incorporating Ground Blast-Furnace Slag and Steel Slag[J]. *Construction and Building Materials*, 2022, 344: 128 265

[59] Schöler A, Lothenbach B, Winnefeld F, *et al*. Hydration of Quaternary Portland Cement Blends Containing Blast-Furnace Slag, Siliceous Fly Ash and Limestone Powder[J]. *Cement and Concrete Composites*, 2015, 55: 374-382

[60] Habert G, Denarié E, Šajna A, *et al*. Lowering the Global Warming Impact of Bridge Rehabilitations by Using Ultra High Performance Fibre Reinforced Concretes[J]. *Cement and Concrete Composites*, 2013, 38: 1-11

[61] Yang R, Yu R, Shui Z, *et al*. Low Carbon Design of an Ultra-High Performance Concrete (UHPC) Incorporating Phosphorous Slag[J]. *Journal of Cleaner Production*, 2019, 240: 118 157

[62] Zhang T, Sun Z, Yang H, *et al*. Enhancement of Triisopropanolamine on the Compressive Strength Development of Cement Paste Incorporated with High Content of Wasted Clay Brick Powder and Its Working Mechanism[J]. *Construction and Building Materials*, 2021, 302: 124 052